ACS APPLIED MATERIALS & INTERFACES

Research Article

www.acsami.org

Vapor–Solid Growth of p-Te/n-SnO_2 Hierarchical Heterostructures and Their Enhanced Room-Temperature Gas Sensing Properties

Yung-Chiun Her,* Bu-Yu Yeh, and Sing-Lin Huang

Department of Materials Science and Engineering, National Chung Hsing University, Taichung 40227, Taiwan

Supporting Information

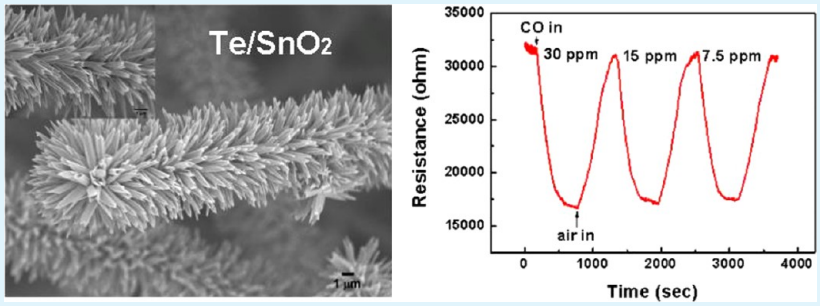

ABSTRACT: We have synthesized brushlike p-Te/n-SnO_2 hierarchical heterostructures by a two-step thermal vapor transport process. The morphologies of the branched Te nanostructures can be manipulated by adjusting the source temperature or the argon flow rate. The growth of the branched Te nanotubes on the SnO_2 nanowire backbones can be ascribed to the vapor–solid (VS) growth mechanism, in which the inherent anisotropic nature of Te lattice and/or dislocations lying along the Te nanotubes axis should play critical roles. When exposed to CO and NO_2 gases at room temperature, Te/SnO_2 hierarchical heterostructures changed the resistance in the same trend and exhibited much higher responses and faster response speeds than the Te nanotube counterparts. The enhancement in gas sensing performance can be ascribed to the higher specific surface areas and formations of numerous Te/Te or TeO_2/TeO_2 bridging point contacts and additional p-Te/n-SnO_2 heterojunctions.

KEYWORDS: *p-Te/n-SnO_2, hierarchical heterostructures, vapor phase process, growth mechanism, room-temperature gas sensor*

1. INTRODUCTION

Recently, three-dimensional (3D) hierarchical heterostructures have drawn great attention due to their rich architectures, distinct properties, and various novel applications.[1−3] Generally, nanoscale 3D hierarchical heterostructures are assembled from two different materials with low-dimensional nanostructures, such as nanoparticles, nanorods, nanowires, nanotubes, nanobelts, and nanosheets. Such complex nanoscale heterostructures can provide an ultrahigh specific surface area and a network system consisting of parallel connective paths and interconnections of dissimilar functional components so that the performance of potential applications can be significantly enhanced.[4−6]

Semiconducting metal oxides, especially SnO_2, have been commonly used as the active sensing materials for gas sensors due to their high sensitivity and selectivity to the ambient conditions.[7] Therefore, various 3D hierarchical heterostructures using the SnO_2 nanowire as a template, such as $W_{18}O_{49}$,[8] NiO,[9] ZnO,[10] and In_2O_3[11] branched nanowires on SnO_2 nanowire backbones, were synthesized for gas sensor applications. Although these sensing materials exhibit enhanced sensitivities to low-concentration chlorine (Cl_2), hydrogen (H_2), ethanol (C_2H_5OH), and carbon monoxide (CO), the integrated gas sensors normally function at high temperatures (250−400 °C) to promote the adsorption and desorption kinetics of surface molecules so that the influence of the resultant heating on the adjacent components as well as high power consumption are still the crucial issues when gas sensors based on hierarchical heterostructures are integrated into microelectronics and portable devices.[12] Besides, high operating temperature is detrimental to the long-term stability of gas sensor devices. Thus, it is of necessity to develop a gas sensor operable at room temperature that will have many benefits, for instance, long device lifetime, simple configuration, low power consumption, and reduced explosion threats.[13]

Tellurium (Te) is a direct band gap, p-type chalcogenide semiconductor with a band gap energy of 0.35 eV. Owing to its unique and interesting properties, Te has been widely used in optical storage medium,[14] high-efficiency photoconductors,[15] piezoelectric[16] and thermoelectric[17] devices, as well as gas sensors.[18−21] For use in gas sensors, Te thin films showed promising sensing properties at room temperature for several poisonous gases, such as propylamine,[18] carbon monoxide (CO),[18] nitrogen dioxide (NO_2),[19] ammonia (NH_3),[20] and hydrogen sulfide (H_2S).[21] Further improvements in sensitivity to NO_2 gas[22] and selectivity to chlorine gas[23] were reported in

Received: March 1, 2014
Accepted: May 22, 2014
Published: May 22, 2014

   dx.doi.org/10.1021/am5012518 | ACS Appl. Mater. Interfaces 2014, 6, 9150−9159

one-dimensional (1D) Te nanotubes due to their high specific surface areas. In our previous work, we also reported that Te nanotubes demonstrate suitable sensitivities, quick response and recovery speeds, and the same trend in resistance change when exposed to CO and NO_2 gases at room temperature.[24] These distinctive properties make Te a favorable candidate that can be used in air-quality sensors with a single sensing material. Compared with one-dimensional Te nanotubes, 3D hierarchical heterostructures, assembled from Te and other n-type metal oxides, not only can provide an even higher surface-to-volume ratio but also can form more bridging point contacts between the electrodes and heterojunctions between the backboned and the branched nanostructures. It is expected that 3D p-Te/n-SnO_2 hierarchical heterostructures will display a considerably enhanced gas sensing performance at room temperature in many aspects, such as the sensitivity, the response and recovery times, the selectivity, and the lowest detectable concentrations.

For the growth of 3D hierarchical heterostructures, the thermal vapor transport process and hydrothermal method are two important synthetic approaches. Although the hydrothermal method provides a simple, inexpensive, environmentally friendly, low-temperature, and high-throughput chemical route, the two-step thermal vapor transport process is frequently adopted because one can accurately control the crystallinities and compositions of the hierarchical heterostructures through the thermal evaporation steps.[6] In this work, we synthesized p-Te/n-SnO_2 hierarchical heterostructures by a two-step thermal vapor transport process. The SnO_2 nanowire cores were synthesized by using a typical Au-catalytic vapor−liquid−solid (VLS) growth process in the first step, and then the Te nanotube branches were subsequently grown onto the SnO_2 nanowire cores by using a vapor−solid (VS) growth process in the second step. To investigate the mechanism for the growth of the secondary Te branched nanostructures, we intentionally interrupted the growth process at different times to monitor their structural evolution. The room-temperature gas sensing properties of p-Te/n-SnO_2 hierarchical heterostructures for CO and NO_2 gases were measured and compared to the Te nanotube counterparts. The possible reasons for their significant enhancement of sensing performance to CO and NO_2 gases were explored.

2. EXPERIMENTAL SECTION

Synthesis of brushlike p-Te/n-SnO_2 hierarchical heterostructures was conducted using a two-step thermal vapor transport process. In the first step, SnO_2 cored nanowires were grown by a typical Au-catalytic VLS process. An alumina boat loaded with 1.0 g of Sn powders (99.99%) was positioned at the center of a horizontal quartz tube furnace with three heating zones. For convenience, we named zones A, B, and C from the inlet to the outlet. A Si substrate covered with an Au film of 10 nm in thickness was positioned at 4 cm from the alumina boat at the downstream side. The temperatures of zones A, B, and C were increased to 860 °C at a heating rate of 20 °C min^{-1} and held at this temperature for 30 min. Argon (Ar) flowed at a rate of 100 cm^3(STP) min^{-1} with a trace amount of oxygen, maintaining the tube pressure at ∼1 Torr during growth. After the growth of SnO_2 nanowire cores, an alumina boat filled with 0.7 g of tellurium powders (99.99%) was placed at the center (zone B) of the quartz tube, while the Si substrate covered with the pregrown SnO_2 nanowires was situated near the end of zone C, approximately 30 cm downstream from the alumina boat. The temperatures of the tubular furnace were increased to 560 °C at zones A and B and 460 °C at zone C in the presence of argon flow (100 cm^3(STP) min^{-1}) at ∼1 Torr and then held for 40 min. It should be noted that the growth substrate was intentionally positioned near the left end of the tubular furnace to create an adequate temperature drop. Because of the fully developed laminar flow in the tube, the actual temperature at substrate should be lower than the setting temperature and was measured to be 115 °C. To understand the effects of process parameters on the Te branched nanostructures, the source (zone B) temperature and argon flow rate were changed. The temperature at zone A was set to be the same as that at zone B. To investigate the mechanism for the growth of the branched Te nanostructures, we interrupted the growth process in the second step at different growth times to observe their morphological changes. The morphologies and crystalline structures of the as-grown products were characterized by field-emission scanning electron microscope (FE-SEM), transmission electron microscope (TEM), and X-ray diffraction (XRD) using Cu Kα (λ = 0.15405 nm) radiation. For study of gas sensing properties, the as-synthesized Te/SnO_2 hierarchical heterostructures were mixed with methanol under ultrasonic treatment to form a homogeneous suspension, which was then distributed on the Al_2O_3 substrate with interdigitated electrodes with a gap size of 0.12 mm between two fingers. The interdigitated electrodes were fabricated by screen-printing silver conductive paste on the Al_2O_3 substrate. Supporting Information Figure S1a displays an optical microscope (OM) image of an alumina substrate with interdigitated silver paste electrodes, and Supporting InformationFigure S1b shows a typical SEM image of the percolating Te/SnO_2 hierarchical heterostructures in the as-fabricated gas sensor (please see the Supporting Information). The as-fabricated gas sensors were then heat-treated at 180 °C for 16 h in an ambient atmosphere in order to further improve the contact properties between the Te/SnO_2 hierarchical heterostructures and the silver paste electrodes. The measurements of gas sensing properties were conducted in a quartz tube, and synthetic air mixed with the desired concentration of CO or NO_2 was introduced at room temperature. The humidity in the quartz tube was measured to be ∼54% relative humidity (RH). The dynamic electrical responses of the gas sensors based on the Te/SnO_2 hierarchical heterostructures were monitored by a volt−amperometric method, where a constant bias of 5 V was applied, and the variations of resistance of gas sensors with time were recorded using a multimeter (Keithley 2410).

3. RESULTS AND DISCUSSION

Typical FE-SEM image and XRD patterns of the as-synthesized products prepared in the first step are shown in Figure 1a,b. It can be seen that large-scale nanowires with lengths of a few tens of micrometers and widths of 200−300 nm were obtained. All of the X-ray diffraction peaks correspond to the tetragonal rutile SnO_2 phase with lattice parameters of a = 0.474 nm and c = 0.319 nm, which are consistent with the standard data file (JCPDS file no. 88-0287). The as-grown SnO_2 nanowires then served as the templates for the subsequent growth of the secondary Te branched nanostructures to form Te/SnO_2 hierarchical heterostructures.

FE-SEM micrographs of the as-synthesized samples obtained in the second step at various source (zone B) temperatures and an actual substrate temperature of 115 °C are shown in Figure 2a−c. At a source temperature of 460 °C, the SnO_2 nanowire backbones were found to be fully covered by Te thin layers with many flakelike Te nanostructures (nanoflakes) growing out of the surfaces. There are few tellurium powders still remaining in the alumina boat, representing that tellurium source powders were evaporated incompletely. When the source temperature was set to 560 °C, tellurium source powder was found to be completely evaporated, and numerous dense tubular Te nanostructures (nanotubes) with widths of about 500−600 nm and lengths of a few micrometers had grown out and completely coved the SnO_2 nanowire backbones to form brushlike Te/SnO_2 hierarchical heterostructures. When we further increased the source temperature to 660 °C, solid Te

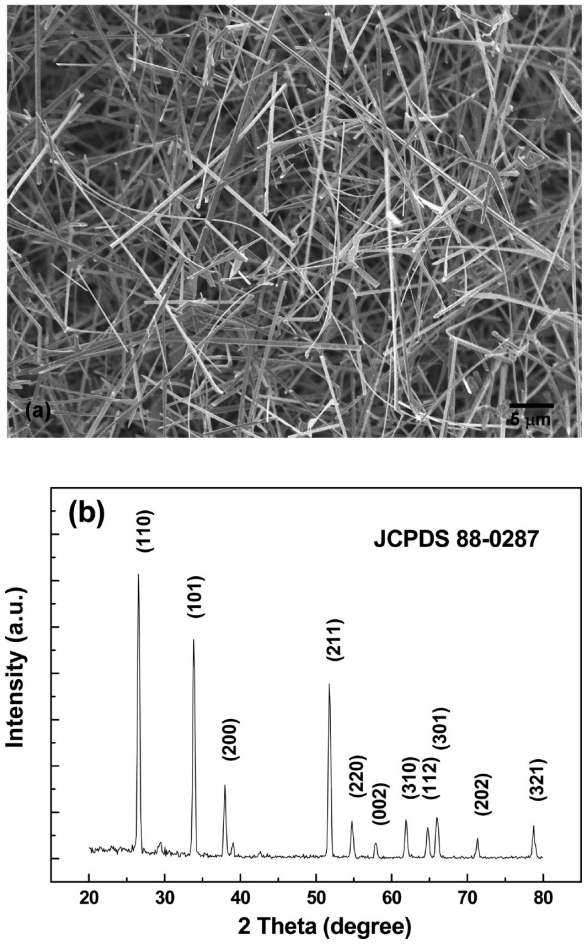

Figure 1. (a) FE-SEM image and (b) XRD patterns of the as-synthesized products prepared in the first step.

micropillars with widths of about 500−800 nm and lengths of several micrometers would grow out of the SnO_2 nanowire backbones. Evidently, the morphologies of the branched Te nanostructures were significantly affected by the source temperature and would transform from nanoflakes to nanotubes and to micropillars when the source temperatures were elevated. Parts a−c of Figure 3 reveal typical FE-SEM micrographs of the as-synthesized samples obtained in the second step under argon flow rates of 50, 100, and 200 cm^3(STP) min^{-1}. Here the source and actual substrate temperatures were controlled at 560 and 115 °C, respectively. It can be seen that micropillars, nanotubes, and screenlike nanostructures (nanoscreens) were grown out of the SnO_2 nanowire backbones as the argon flow rates were kept at 50, 100, and 200 cm^3(STP) min^{-1}, respectively. The effect of the argon flow rate on the morphologies of the branched Te nanostructures was found to be opposite to that of the source temperature. Nevertheless, we can easily control the morphologies of the branched Te nanostructures by simply adjusting the source temperature or the argon flow rate.

It is known that the degree of supersaturation of the source vapor plays a dominant role in the resultant growth morphology as nanostructures were grown by a vapor transport method.[25] To grow 1D nanostructures, the degree of supersaturation should be controlled below a threshold level. Once the supersaturation is above the threshold level, one will obtain bulk crystals or powders. Normally, the supersaturation

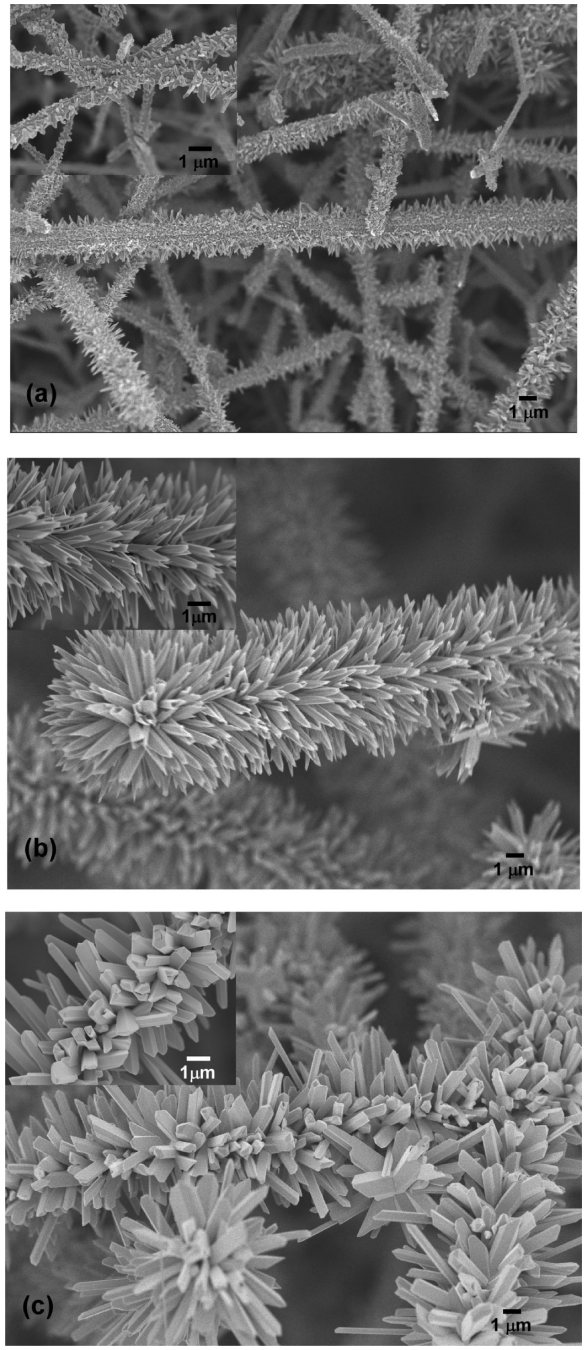

Figure 2. FE-SEM images of the as-grown products prepared at source temperatures of (a) 460, (b) 560, and (c) 660 °C, a substrate temperature of 115 °C, and a gas flow rate of 100 cm^3(STP) min^{-1} for 40 min.

ratio (α) of a source vapor can be expressed as $\alpha = P/P_0$, where P is the source vapor pressure close to the substrate and P_0 is the vapor pressure of condensed solid at the substrate. It has been reported by Johnson et al. that in a tubular furnace the carrier gas temperature not is only affected by furnace temperature, gas flow rate, and reactor pressure but also is a function of axial and radial position because of the fully developed laminar flow in the tube.[26] It is also reported that the relationship between the saturated vapor pressure of Te (P_{Te}) and the absolute temperature (T) is described as $\log(P_{Te}) = 7.6 - (5960.2/T)$.[27] To understand the influences of source temperature and argon gas flow rate on the resultant

dx.doi.org/10.1021/am5012518 | ACS Appl. Mater. Interfaces 2014, 6, 9150−9159

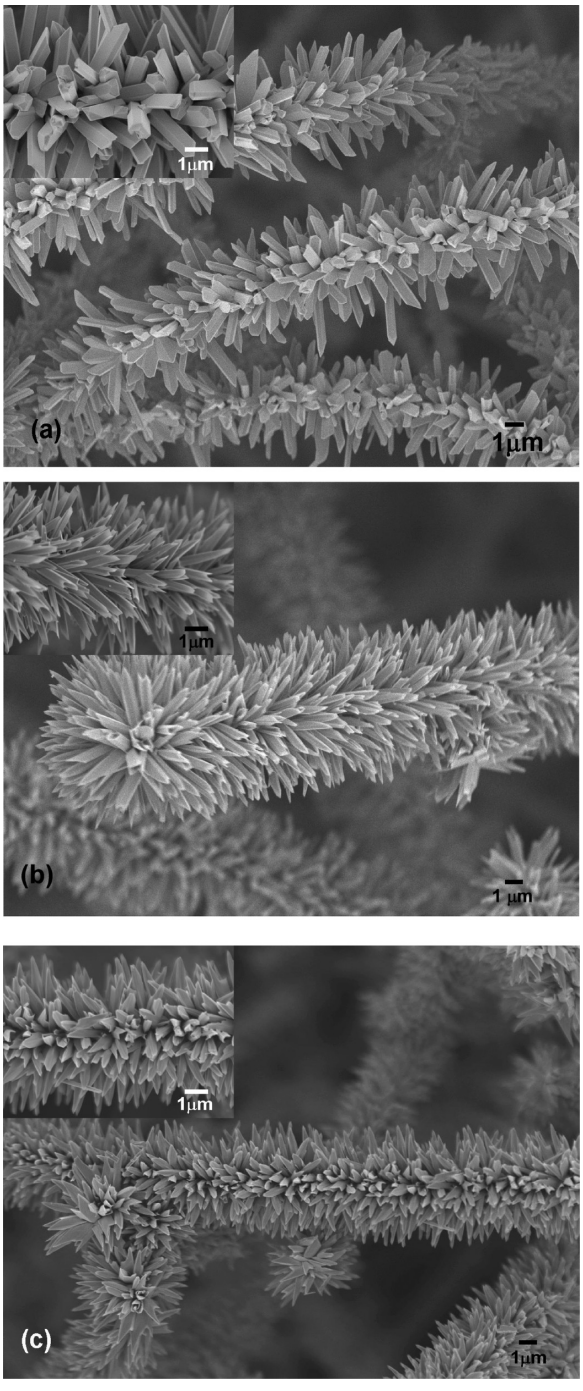

Figure 3. FE-SEM images of the as-grown products prepared under gas flow rate of (a) 50, (b) 100, and (c) 200 cm^3(STP) min^{-1} at a source temperature of 560 °C and a substrate temperature of 460 °C for 40 min.

morphologies of the branched Te nanostructures, the α values of tellurium vapor at the alumina substrate at different growth conditions need to be estimated. Because the furnace temperature at zone C was fixed to 460 °C, and zone B was controlled at 460, 560, and 660 °C, the measured temperatures at the center of the quartz tube above the alumina substrate were 208, 215, and 226 °C, respectively, while that on the substrate was kept at ∼115 °C, giving rise to the α values of about 933, 1405, and 2612, respectively. The calculated α values fall in the range of α = 174−3528, which are calculated from the growth temperatures reported by Furuta et al. where they grew different types of 1D tellurium whiskers.[28] This can explain the growth of 1D Te branched nanostructures in this work. Additionally, the α value is found to increase with increasing source temperature. That means more Te vapor atoms will condense on the growth substrate surface at a higher source temperature so that the resultant Te branched nanostructures will transform from nanoflakes to nanotubes, and to micropillars when we raised the zone B (source) temperature. Considering the influence of argon flow rate, Johnson et al. also pointed out that the real temperature inside a quartz tube will not be able to reach the furnace temperature at any axial position as the flow rate of carrier gas exceeds a threshold value.[26] It is reasonable to suggest that once the source and actual substrate temperatures were kept constant, more heat can be transported downstream to the growth substrate when the argon flow rate is low so that a higher carrier gas temperature can be reached, leading to a higher supersaturation ratio. That can explain why the resultant Te branched nanostructures transformed from micropillars to nanotubes, and to nanoscreens when the argon flow rate was increased from 50 to 100, and then to 200 cm^3(STP) min^{-1}.

Figure 4a displays XRD patterns of the as-grown products obtained in the second step at a source temperature of 560 °C and an actual substrate temperature of 115 °C. All diffraction peaks were successfully indexed with the assumption of a hexagonal crystal structure of Te (JCPDS file no. 36-1452). No diffraction peaks corresponding to tin oxides or tellurium oxides were found, suggesting that the SnO_2 nanowire backbones have been completely covered by Te and the branched nanotubes contain only Te. The crystalline structure and growth direction of the branched nanostructures were further characterized using TEM analysis. Figure 4b shows a TEM bright-field image of a representative Te/SnO_2 hierarchical heterostructure obtained at the initial stage. It can be seen that the SnO_2 nanowire core was covered by a thin Te layer, and several Te nanoflakes had grown out of the surface. As we closely examined the structure of a protruded nanoflake, the magnified TEM image and selected area electron diffraction (SAED) patterns, as shown in Figure 4c, confirm that those protruded nanoflakes are single-crystalline hexagonal Te and grow along the [0001] direction. Figure 4d displays the TEM image and the SAED patterns of the branched nanotubes stripped from the as-synthesized hierarchical heterostructures. Clearly, tubular nanostructures were grown from the SnO_2 nanowire backbones, and the regular SAED spots approve that single-crystalline Te branched nanotubes growing along the *c*-axis were obtained in the second step.

To reveal how the Te branched nanotubes grow from the SnO_2 nanowire backbones, the synthesis processes were interrupted at different growth times to carefully observe the morphological evolution of the products. Here the growth times were counted from the start of the heating process. Parts a−f of Figure 5 illustrate the FE-SEM micrographics of the samples obtained after interrupting the growth process at various times. At the heating time of 14 min, there is no discernible nanostructure, as shown in Figure 5a. Once the heating time reached 16 min, the SnO_2 nanowire backbone was fully covered by a thin tellurium layer to form a rough surface decorated with many nanoparticles (Figure 5b). Some nanospikes were found to grow out of the rough surface. At the heating time of 20 min, the Te surface layer became thicker and rougher, and the nanospikes multiplied and grew up

dx.doi.org/10.1021/am5012518 | ACS Appl. Mater. Interfaces 2014, 6, 9150−9159

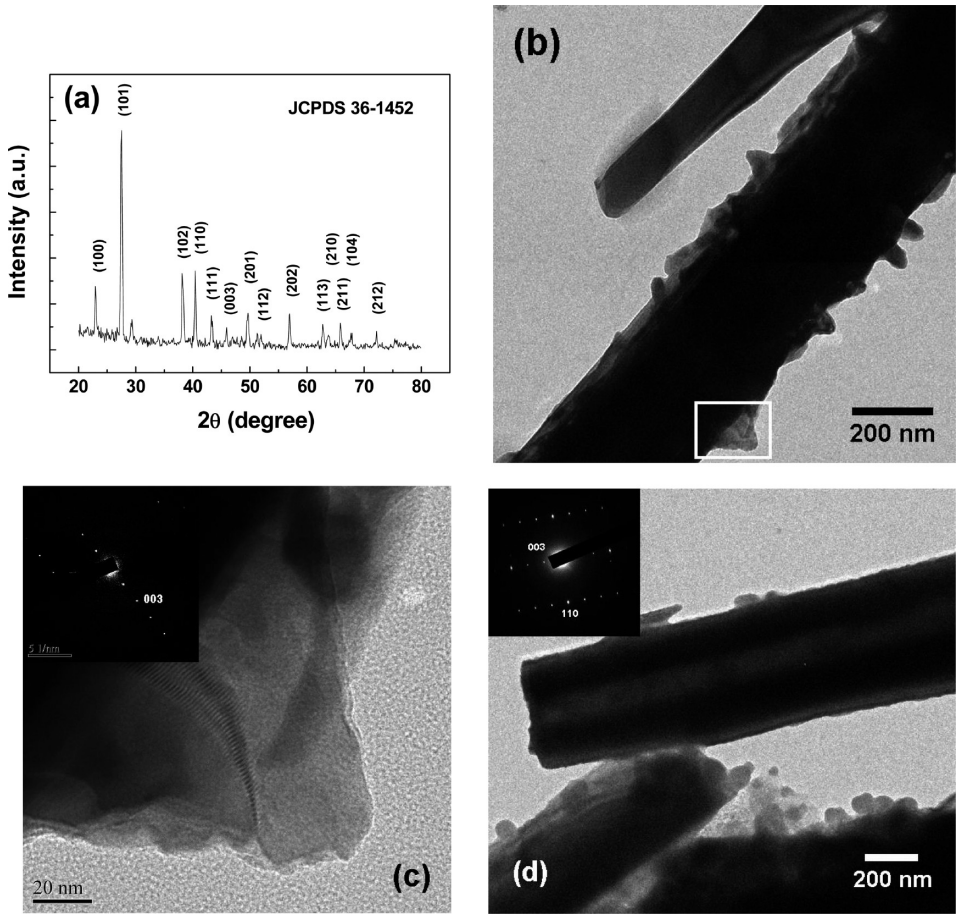

Figure 4. (a) XRD patterns of the as-synthesized hierarchical nanostructures, (b) TEM image of a Te/SnO_2 hierarchical nanostructure obtained at the initial stage, (c) magnified TEM image and SAED patterns taken from the square area of panel b, and (d) TEM image and SAED patterns of Te nanotubes stripped from Te/SnO_2 hierarchical nanostructures.

(Figure 5c). At the heating time of 28 min, both zones B and C had reached their desired temperatures, and nanospikes developed into protruded nanoflakes (Figure 5d). As the incoming Te source atoms would be preferentially absorbed at the protuberances of nanoflakes, the protruded nanoflakes grew out of the surfaces of the SnO_2 nanowire cores in the perpendicular directions. After the tubular furnace was heated to the desired temperature and the temperature was retained 10 more min, the protruded nanoflakes continuously grew and some of them had developed toward V-grooved nanoscreens (Figure 5e). Once the retaining time reached 30 min, most protruded nanoflakes had developed into V-grooved nanoscreens, which completely covered the surface of the SnO_2 nanowire backbone (Figure 5f). It is worth noting that when the holding time was extended further to 40 min, the constant supply of Te source atoms would lead to not only the longitudinal growth at the tips, but also the lateral growth at the bases so that the V-grooved nanoscreens developed into intermediary nanotubes, which have unclosed segments at the ends, as shown in Figure 2b.

According to the observed structural evolution, the growth of the Te branched nanostructures on the SnO_2 nanowire backbones by a thermal vapor transport process can be attributed to the VS growth mechanism as no metal catalysts were used. In addition, the inherent anisotropic nature of the Te lattice and/or dislocations lying along the Te nanotubes axis should play critical roles.[28,29] When the source temperature is increased to a sufficient value, the vaporization of Te metal powders will generate a substantial amount of Te vapor atoms that are then transported downstream to the growth substrate. The deposition of Te vapor atoms on the surfaces of SnO_2 nanowire backbones will form a rough Te thin layer decorated with many nanoparticles in the initial stage. As more Te vapor atoms are conveyed to the SnO_2 nanowire backbones, Te nanoparticles in a preferred orientation will grow fast and gradually develop into Te nanospikes and nanoflakes with their growth directions normal to the surfaces of SnO_2 nanowire backbones. Because the $\{10\bar{1}0\}$ planes have a much lower surface free energy than other prismatic surfaces, and Te has a strong anisotropic character, $(10\bar{1}0)$ Te nanoflakes will form and grow along the [0001] direction. When Te vapor atoms are constantly fed to the preexisting Te nanoflakes, they will not only continuously grow in the longitudinal direction but also gradually grow in the lateral direction to form other low-energy $\{10\bar{1}0\}$ planes, leading to the progressive developments of Te nanoflakes into V-grooved nanoscreens, four-face nanogrooves, and intermediary nanotubes consisting of $\{10\bar{1}0\}$ planes. The schematic illustration of the growth mechanism of Te branched nanotubes on the SnO_2 nanowire backbones by a thermal vapor transport process is shown in Figure 6.

The resistance of the Te/SnO_2 hierarchical heterostructures as a function of time when exposed to different concentrations of CO and NO_2 gases are shown in Figure 7a,b, respectively. It was found that the resistance of the Te/SnO_2 hierarchical

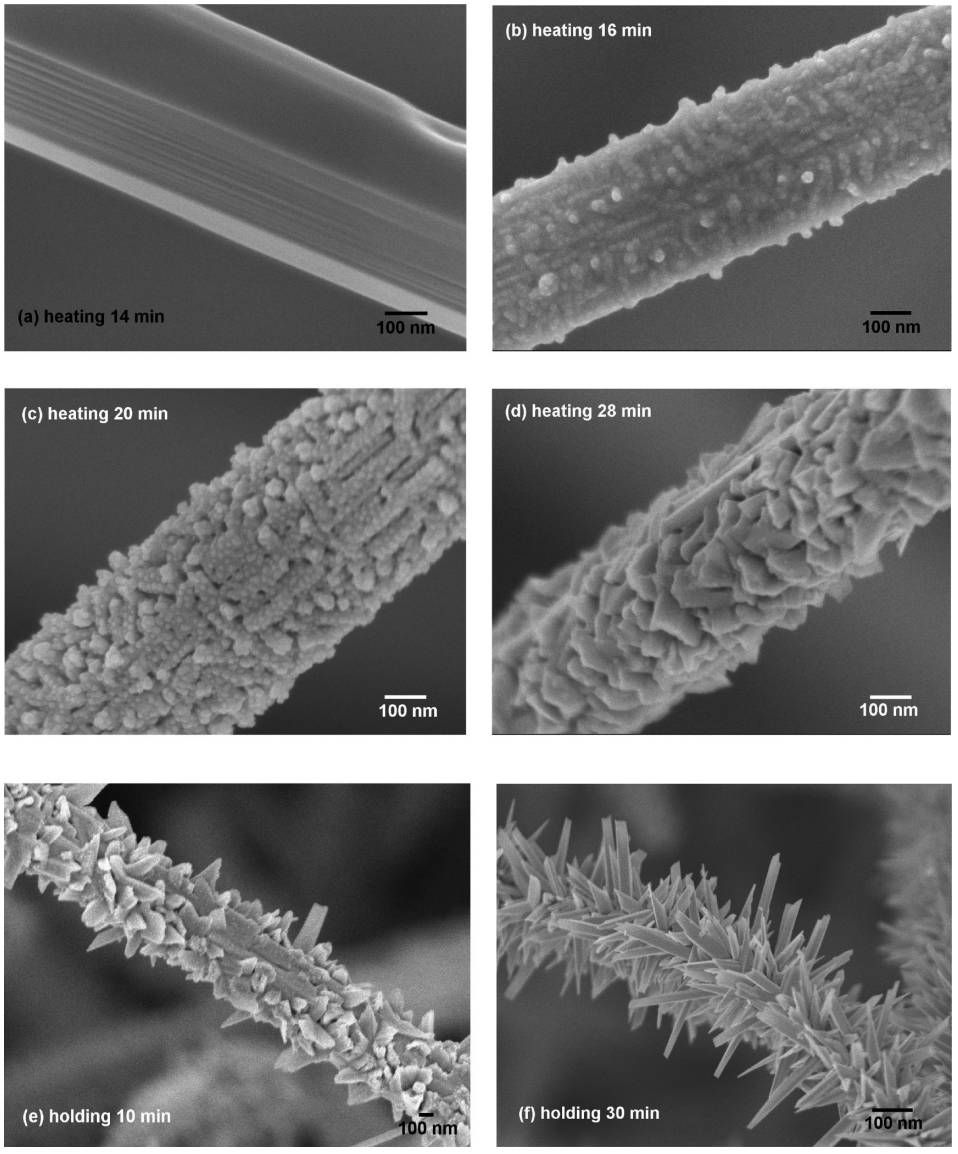

Figure 5. FE-SEM images of the as-synthesized products at heating times of (a) 14, (b) 16, (c) 20, and (d) 28 min and holding times of (e) 10 and (f) 30 min.

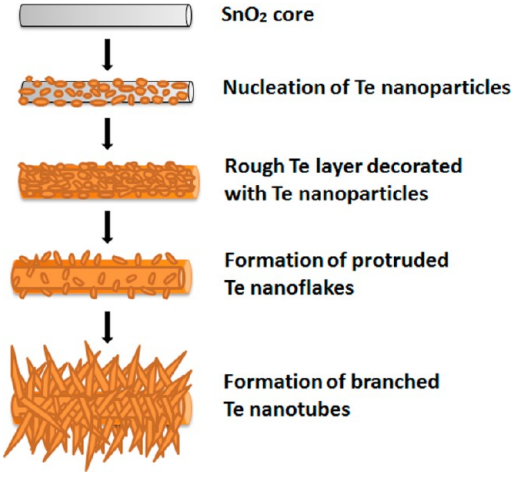

Figure 6. Schematic illustrations for the growth mechanisms of branched Te nanotubes on the SnO_2 nanowire backbones.

heterostructure gas sensors decreased when CO and NO_2 gases were introduced. Once we turned off the test gases, the resistance increased almost back to its original value. Apparently, the Te/SnO_2 hierarchical heterostructures changed the resistance in the same trend when exposed to both the reducing CO and oxidizing NO_2, and the absorption and desorption processes of the tested gases are reversible. Here, we defined the gas response as the ratio of the resistance in air (R_a) to the resistance in the presence of test gas (R_g). The response and recovery times were defined as the times taken to reach 90% of steady-state values of the resistance change. When the Te/SnO_2 hierarchical heterostructures were exposed to CO with concentrations of 30, 15, and 7.5 ppm, the responses were about 1.89, 1.83, and 1.79, the response times were 263, 343, and 372 s, and the recovery times were 463, 420, and 349 s, respectively. Upon exposure to 15, 7.5, and 3 ppm NO_2 gases, the responses were about 8.52, 7.16, and 6.53, the response times were 132, 243, and 294 s, and the recovery times were 1178, 889, and 709 s, respectively. Parts a and b of Figure 8 display the room-temperature response transients of bare Te

dx.doi.org/10.1021/am5012518 | ACS Appl. Mater. Interfaces 2014, 6, 9150−9159

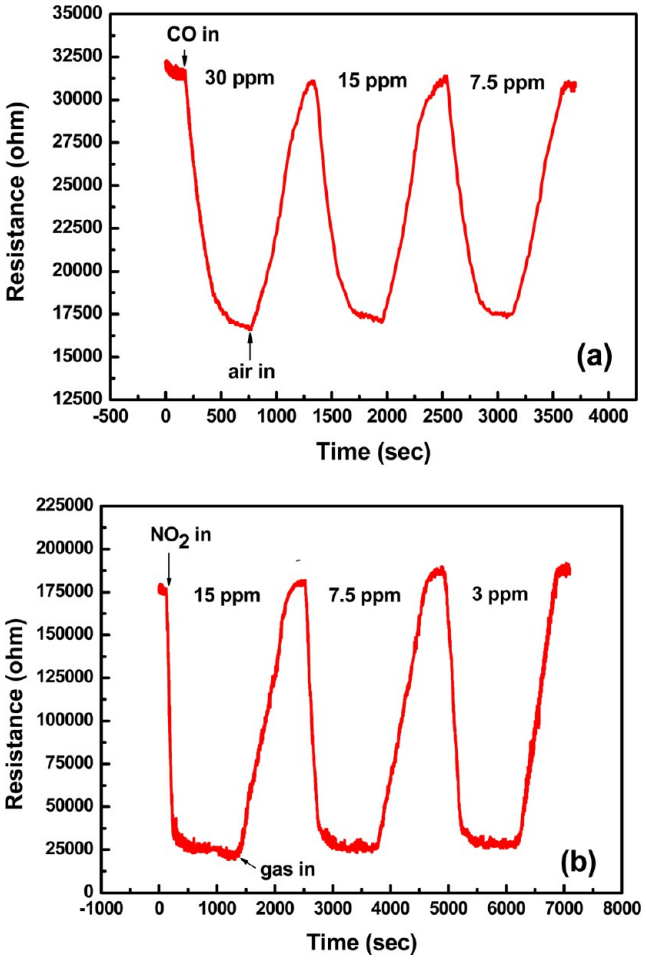

Figure 7. Dynamic gas responses of Te/SnO_2 hierarchical heterostructures to (a) CO and (b) NO_2 with various concentrations at room temperature.

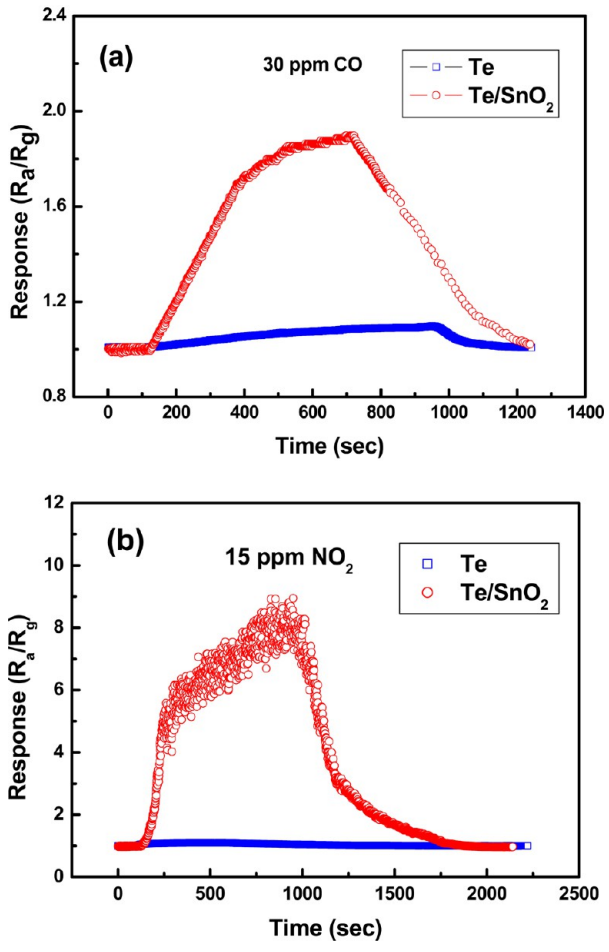

Figure 8. Response transients of bare Te nanotubes and Te/SnO_2 hierarchical heterostructures to (a) 30 ppm CO and (b) 15 ppm NO_2 at room temperature.

nanotubes and Te/SnO_2 hierarchical heterostructures to 30 ppm CO and 15 ppm NO_2 gases, respectively. It is worthy of note that bare SnO_2 nanowires had no response to both CO and NO_2 at room temperature in the present work. Compared with bare Te nanotubes, Te/SnO_2 hierarchical heterostructures show significantly higher responses and shorter response times when exposed to CO and NO_2 gases. The responses of Te/SnO_2 hierarchical heterostructures to 30 ppm CO and 15 ppm NO_2 are about 1.7 and 7.7 times, respectively, of those of bare Te nanotubes.

In Figure 7a,b, we also found that the response of the sensor based on Te/SnO_2 hierarchical heterostructures only slightly decreased with decreasing the CO concentration. Normally, when the concentration of test gas increases, the sensor response increases first and then reaches a saturation value. The dependence of sensor response on the gas concentration can be described by a power law and will switch from zero order to first order when the gas concentration is below a threshold value.[30] In the present work, it is believed that the CO concentration of 7.5 ppm should be well above the response threshold of the Te/SnO_2 hierarchical heterostructures, leading to a slight change of gas response with the CO concentration. It should also be mentioned that our measurements of gas sensing properties were conducted in an environmental humidity of 54% RH. Normally, a metal oxide gas sensor will exhibit a lower response in an environment of high humidity.[31] When water molecules are absorbed on the surface of metal oxide, they will react with the absorbed oxygen ions so that the gas sensor resistance in pure air and tested gas ambiences decreases, giving rise to the reduction of gas response.[31] Accordingly, our sensors are expected to exhibit a higher sensitivity at RH < 54% and a lower sensitivity at RH > 54%. To clarify the effect of humidity on our p-Te/n-SnO_2 NWs-based gas sensors, a systematic study needed to be made. It is also noteworthy that stability is another important factor for gas sensors. We also measured the gas responses of p-Te/n-SnO_2 hierarchical heterostructures to 30 ppm CO and 15 ppm NO_2 at room temperature under repeated switching on−off the tested gases for several cycles. No noticeable drifts of the gas responses and response and recovery times were observed, providing evidence that gas sensors based on the Te/SnO_2 hierarchical heterostructures exhibit good stability.

Normally, the resistance of a semiconducting gas sensing material changes in opposite direction upon exposure to reducing and oxidizing gases. However, the resistance of p-Te/n-SnO_2 hierarchical heterostructures decreases upon exposure to both CO and NO_2. Similar results have also been reported by Tsiulyanu et al.[18,19] They suggested that both CO and NO_2 act as acceptors, which tie up the electrons. The surface of the films becomes enriched with holes, leading to the decrease in resistance. They also suggested that no depletion region is formed on the Te film surface before, as in the case of metal

dx.doi.org/10.1021/am5012518 | ACS Appl. Mater. Interfaces 2014, 6, 9150−9159

oxide semiconductors. However, no additional experimental evidence was provided to support their proposed mechanism. Besides, the fabrication process of our gas sensors is different from theirs. In the present work, the as-fabricated gas sensors were heat-treated at 180 °C for 16 h in an ambient atmosphere in order to further improve the contact properties between the Te/SnO_2 hierarchical heterostructures and the silver paste electrodes. In our previous work,[24] we have confirmed that the oxidation of Te nanotubes occurs after the as-fabricated Te nanotube gas sensor was heated at 180 °C for 16 h, and a thin TeO_2 layer will be formed on the top surfaces of Te nanotubes. We also found that the preexisting TeO_2 will convert back to Te after exposure to CO; meanwhile, the TeO_2 layers will become thicker after exposure to NO_2. Sen et al. also observed the reduction of TeO_2 to Te in the Te film with a TeO_2 surface layer upon exposure to H_2S.[21] Similar oxidization and reduction reactions are expected to occur in Te/SnO_2 hierarchical heterostructures. Therefore, the effect of the formation of the TeO_2 surface layer on the total resistance of gas sensors should also be taken into consideration.

For our gas sensors based on Te/SnO_2 hierarchical heterostructures, a percolating network will be formed between two adjacent finger electrodes, and the conductivity between two electrodes is determined by the availability of the conducting paths through the percolating network.[10] Since the SnO_2 nanowire backbones have been fully covered by Te thin films and Te branched nanotubes, the total resistance of the gas sensor can be considered to be mainly contributed from the resistance of Te coated SnO_2 nanowire cores and Te branched nanotubes associated with the resistance at the bridging contact points. As mentioned earlier, TeO_2 surface thin layers are expected to form on the Te coated SnO_2 nanowire cores and Te nanotube branches after the as-fabricated gas sensors were heated at 180 °C for 16 h. It is known that Te and TeO_2 belong to so-called lone-pair (LP) semiconductor materials.[32,33] TeO_2 has a significantly higher resistivity than Te.[34] Hole-enriched regions will be expected to form on the TeO_2 surface layer and the surfaces of Te branched nanotubes. When gas sensors based on Te/SnO_2 hierarchical heterostructures are exposed to an ambient atmosphere at room temperature, oxygen molecules absorbed on the TeO_2 surface layers and surfaces of Te branched nanotubes act as acceptor sites and trap LP electrons from O_2^-, resulting in the increase in hole concentration as well as conductivity. When Te/SnO_2 hierarchical heterostructures are exposed to the reducing CO, CO can be oxidized by O_2^- ions and reduce TeO_2 to metallic Te at the same time. The oxidization of CO by O_2^- ions releases electrons back to the TeO_2 coated Te branched nanotubes and decrease the number of surface O_2^-; that will reduce the hole concentration and therefore raise the resistance of Te coated SnO_2 nanowire cores and Te branched nanotubes, and the resistance at the contact points. In contrast, the reduction of TeO_2 to metallic Te can also diminish the above resistance. We believe that the reduction of TeO_2 to metallic Te plays a dominant role over the oxidization of CO by O_2^- ions so that the resistance of Te/SnO_2 hierarchical heterostructure gas sensor decreases when exposed to the reducing CO. When Te/SnO_2 hierarchical heterostructures are exposed to the oxidizing NO_2, NO_2 molecules can facilitate the oxidation of Te nanotubes to form a thicker TeO_2 layer, so that the resistance of Te branched nanotubes themselves and the resistance at contact points slightly increase. Meanwhile, NO_2 molecules, behaving like dangling bonds, can also accept the lone-pair electrons in Te and TeO_2,[23] leading to the increase in hole concentration and thus the decrease in resistance of TeO_2 covered SnO_2 nanowire cores and Te nanotube branches. Apparently, the acceptor-like character of NO_2 molecules exhibits a stronger effect than the thickening of TeO_2 layers caused by oxidation so that the resistance of our Te/SnO_2 hierarchical heterostructure gas sensor decreases when exposed to the oxidizing NO_2. These explain the same direction of resistance change of our Te/SnO_2 hierarchical heterostructure gas sensor when exposed to the reducing CO and oxidizing NO_2.

Regarding the enhancement in response and response time to CO and NO_2 gases for our Te/SnO_2 hierarchical heterostructures compared with bare Te nanotubes, it may be attributed to their much higher specific surface areas and the formations of numerous Te/Te or TeO_2/TeO_2 bridging point contacts and additional p-Te/n-SnO_2 heterojunctions. Figure S2 (see the Supporting Information) demonstrates the current−voltage (I−V) curves of our Te/SnO_2 hierarchical heterostructure gas sensor acquired in air, 15 ppm NO_2, and 30 ppm CO at room temperature. The nonlinear I−V characteristics suggest that Schottky-type nanowire−nanowire junctions at bridging points and/or built-in potential near the p−n junctions were formed in the Te/SnO_2 hierarchical heterostructures. High specific surface areas of Te/SnO_2 hierarchical heterostructures provide abundant active sites for oxygen and tested gases, leading to a quick and substantial change in the surface hole concentrations, and thus the resistance. The potential barriers at the contact points between Te branched nanotubes and near the p-Te/n-SnO_2 heterojunctions between two adjacent electrodes can effectively modulate the electron transport, and hence the resistance variation of the gas sensor. When p-Te/n-SnO_2 hierarchical heterostructures are exposed to air, oxygen molecules can be more easily absorbed on Te surfaces with the assistance of SnO_2, since the electrons in n-type SnO_2 backbones will transfer to p-type Te branched nanotubes or Te surface layers. This process not only enhances the absorption of oxygen molecules and molecule−ion conversion rate but also increases the width of the depletion region at the p-Te/n-SnO_2 heterojunction, giving rise to the increases in both response and response speed.

4. CONCLUSION

Brushlike p-Te/n-SnO_2 hierarchical heterostructures were synthesized by a two-step thermal vapor transport process. As the source temperatures were increased or the argon flow rates were decreased, the morphologies of the branched Te nanostructures would transform from nanoflakes to hollow nanotubes and to solid micropillars. It can be seen that a rough Te thin layer decorated with many nanoparticles will be formed on the SnO_2 nanowire backbones at the beginning of the growth process, and then gradually grow into Te nanospikes, nanoflakes, V-grooved nanoscreens, and intermediary nanotubes consisting of $\{10\bar{1}0\}$ planes. The VS mechanism should govern the growth of Te branched nanotubes on the SnO_2 nanowire cores in which the inherent anisotropic nature of Te lattice and/or dislocations lying along the Te nanotubes axis should play critical roles. When exposed to CO and NO_2 at room temperature, Te/SnO_2 hierarchical heterostructures changed the resistance in the same trend and exhibit much higher responses and shorter response times than the Te nanotube counterparts. To explain the decrease in resistance of p-Te/n-SnO_2 hierarchical heterostructures upon exposure to

the reducing CO gas, the formation of TeO_2 thin layers during the fabrication process of gas sensor device needs to be taken into consideration. The enhancement in gas sensing performance of our p-Te/n-SnO_2 hierarchical heterostructures may be attributed to the higher specific areas and formations of numerous Te/Te or TeO_2/TeO_2 bridging point contacts and additional p-Te/n-SnO_2 heterojunctions.

■ ASSOCIATED CONTENT

Supporting Information

Figures showing an OM image of an alumina substrate with interdigitated silver paste electrodes, an SEM image of the percolating Te/SnO_2 hierarchical heterostructures in an as-fabricated gas sensor, and $I-V$ curves of the gas sensing device measured in air, 15 ppm NO_2, and 30 ppm CO at room temperature. This material is available free of charge via the Internet at http://pubs.acs.org.

■ AUTHOR INFORMATION

Corresponding Author

*Phone: +886-4-22859112. Fax: +886-4-22857017. E-mail: ycho@dragon.nchu.edu.tw.

Notes

The authors declare no competing financial interest.

■ ACKNOWLEDGMENTS

We would like to acknowledge financial support from the National Science Council (Taiwan, R.O.C.) under Contract No. NSC101-2221-E005-033-MY3.

■ REFERENCES

(1) Whang, D.; Jin, S.; Wu, Y.; Lieber, C. M. Large-Scale Hierarchical Organization of Nanowire Arrays for Integrated Nanosystems. *Nano Lett.* **2003**, *3*, 1255−1259.

(2) Li, B.; Wang, Y. Facile Synthesis and Enhanced Photocatalytic Performance of Flower-like ZnO Hierarchical Microstructures. *J. Phys. Chem. C* **2010**, *114*, 890−896.

(3) Wan, Q.; Huang, J.; Xie, Z.; Wang, T.; Dattoli, E. N.; Lu, W. Branched SnO_2 Nanowires on Metallic Nanowire Backbones for Ethanol Sensors Application. *Appl. Phys. Lett.* **2008**, *92*, 102101-1−102101-3.

(4) Dick, A.; Deppert, K.; Karlsson, L. S.; Larsson, M. W.; Seifert, W.; Wallenberg, L. R.; Samuelson, L. Directed Growth of Branched Nanowire Structures. *MRS Bull.* **2007**, *32*, 127−133.

(5) Niu, M.; Huang, F.; Cui, L.; Huang, P.; Yu, Y.; Wang, Y. Hydrothermal Synthesis, Structural Characteristics, and Enhanced Photocatalysis of SnO_2/α-Fe_2O_3 Semiconductor Nanoheterostructures. *ACS Nano* **2010**, *4*, 681−688.

(6) Thong, L. V.; Loan, L. T. N.; Hieu, N. V. Comparative Study of Gas Sensor Performance of SnO_2 Nanowires and Their Hierarchical Nanostructures. *Sens. Actuators, B* **2010**, *150*, 112−119.

(7) Barsan, N.; Schweizer-Berberich, M.; Gopel, W. Fundamental and Practical Aspects in the Design of Nanoscaled SnO_2 Gas Sensors: A Status Report. *Fresenius' J. Anal. Chem.* **1999**, *365*, 287−304.

(8) Sen, S.; Kanitkar, P.; Sharma, A.; Muthe, K. P.; Rath, A.; Deshpande, S. K.; Kaur, M.; Aiyer, R. C.; Gupta, S. K.; Yakhmi, J. V. Growth of SnO_2/$W_{18}O_{49}$ Nanowire Hierarchical Heterostructure and Their Application as Chemical Sensor. *Sens. Actuators, B* **2010**, *147*, 453−460.

(9) Wang, Z.; Li, Z.; Sun, J.; Zhang, H.; Wang, W.; Zheng, W.; Wang, C. Improved Hydrogen Monitoring Properties Based on p-NiO/n-SnO_2 Heterojunction Composite Nanofibers. *J. Phys. Chem. C* **2010**, *114*, 6100−6105.

(10) Khoang, N. D.; Trung, D. D.; Duy, N. V.; Hoa, N. D.; Hieu, N. V. Design of SnO_2/ZnO Hierarchical Nanostructures for Enhanced Ethanol Gas-Sensing Performance. *Sens. Actuators, B* **2012**, *174*, 594−601.

(11) Her, Y. C.; Chiang, C. K.; Jean, S. T.; Huang, S. L. Self-Catalytic Growth of Hierarchical In_2O_3 Nanostructures on SnO_2 Nanowires and Their CO Sensing Properties. *CrystEngComm* **2012**, *14*, 1296−1300.

(12) Kim, I. D.; Rothschild, A.; Tuller, H. L. Advances and New Directions in Gas-Sensing Devices. *Acta Mater.* **2013**, *61*, 974−1000.

(13) Choi, K. J.; Jang, H. W. One-Dimensional Oxide Nanostructures as Gas-Sensing Materials: Review and Issues. *Sensors* **2010**, *10*, 4083−4099.

(14) Lou, D. Y.; Blom, G. M.; Kenney, G. C. Bit Oriented Optical Storage with Thin Tellurium Films. *J. Vac. Sci. Technol.* **1981**, *18*, 78−86.

(15) Görtz, W.; Gerstenhauer, E.; Grosse, P. Photoconducting Tellurium for Submillimeterwave Detectors. *Appl. Phys. A: Mater. Sci. Process.* **1982**, *27*, 35−38.

(16) Royer, D.; Dieulesaint, E. Elastic and Piezoelectric Constants of Trigonal Selenium and Tellurium Crystals. *J. Appl. Phys.* **1979**, *50*, 4042−4045.

(17) Damodara Das, V.; Jayaprakash, N.; Soundararajan, N. Thermoelectric Power of Tellurium Thin Films and Its Thickness and Temperature Dependence. *J. Mater. Sci.* **1981**, *16*, 3331−3334.

(18) Tsiulyanu, D.; Marian, S.; Liess, H.-D. Sensing Properties of Tellurium Based Thin Films to Propylamine and Carbon Oxide. *Sens. Actuators, B* **2002**, *85*, 232−238.

(19) Tsiulyanu, D.; Marian, S.; Miron, V.; Liess, H.-D. High Sensitive Tellurium Based NO_2 Gas Sensor. *Sens. Actuators, B* **2001**, *73*, 35−39.

(20) Sen, S.; Muthe, K. P.; Joshi, N.; Gadkari, S. C.; Cupta, S. K.; Jagannath; Roy, M.; Deshpande, S. K.; Yakhmi, J. V. Room Temperature Operating Ammonia Sensor Based on Tellurium Thin Films. *Sens. Actuators, B* **2004**, *98*, 154−159.

(21) Sen, S.; Bhandarkar, V.; Muthe, K. P.; Roy, M.; Deshpande, S. K.; Aiyer, R. C.; Cupta, S. K.; Yakhmi, J. V.; Sahni, V. C. Highly Sensitive Hydrogen Sulphide Sensors Operable at Room Temperature. *Sens. Actuators, B* **2006**, *115*, 270−275.

(22) Sen, S.; Sharma, M.; Kumar, V.; Muthe, K. P.; Satyam, P. V.; Bhatta, U. M.; Roy, M.; Gaur, N. K.; Gupta, S. K.; Yakhmi, J. V. Chlorine Gas Sensors Using One-Dimensional Tellurium Nanostructures. *Talanta* **2009**, *77*, 1567−1572.

(23) Siciliano, T.; Filippo, E.; Genga, A.; Micocci, G.; Siciliano, M.; Tepore, A. Single-Crystalline Te Microtubes: Synthesis and NO_2 Gas Sensor Application. *Sens. Actuators, B* **2009**, *142*, 185−190.

(24) Her, Y. C.; Huang, S. L. Growth Mechanism of Te Nanotubes by a Direct Vapor Phase Process and Their Room-Temperature CO and NO_2 Sensing Properties. *Nanotechnology* **2013**, *24*, 215603-1−215603-9.

(25) Xia, Y.; Yang, P.; Sun, Y.; Wu, Y.; Mayer, B.; Gates, B.; Yin, Y.; Kim, F.; Yan, H. One-Dimensional Nanostructures: Synthesis, Characterization, and Applications. *Adv. Mater.* **2003**, *15*, 353−389.

(26) Johnson, D. C.; Morris, W. D.; Prieto, A. Effects of Transport Gradients in a Chemical Vapor Deposition Reactor Employing Vapor−Liquid−Solid Growth of Ternary Chalcogenide Phase-Change Materials. *Nanotechnology* **2010**, *21*, 165604-1−165604-9.

(27) Brooks, L. S. The Vapor Pressures of Tellurium and Selenium. *J. Am. Chem. Soc.* **1952**, *74*, 227−229.

(28) Furuta, N.; Ohasi, Y.; Itinose, H.; Igarashi, Y. Kinetics of Vapor-Grown Tellurium Whiskers. *Jpn. J. Appl. Phys.* **1975**, *14*, 929−934.

(29) Sears, G. W. A Growth Mechanism for Mercury Whiskers. *Acta Metall.* **1955**, *3*, 361−366.

(30) Clifford, P. K.; Tuma, D. T. Characteristics of Semiconductor Gas Sensors I. Steady State Gas Response. *Sens. Actuators* **1982**, *3*, 233−254.

(31) Gong, J.; Chen, Q.; Lian, M.; Liu, N.; Stevenson, R. G.; Adamic, F. Micromachined Nanocrystalline Silver Doped SnO_2 H_2S Sensor. *Sens. Actuators, B* **2006**, *114*, 32−39.

(32) Kastner, M. Bonding Bands, Lone-Pair Bands, and Impurity States in Chalcogenide Semiconductors. *Phys, Rev. Lett.* **1972**, *28*, 355−357.

(33) Champarnaud-Mesjard, J.-C.; Blanchandin, S.; Thomas, P.; Mirgorodsky, A.; Merle-Mejean, T.; Frit, B. Crystal Structure, Raman Spectrum and Lattice Dynamics of a New Metastable Form of Tellurium Dioxide: γ-TeO2. *J. Phys. Chem. Solids* **2000**, *61*, 1499−1507.
(34) Dutton, R. W.; Muller, R. S. Large Grain Tellurium Thin Films. *Thin Solid Films* **1972**, *11*, 229−236.